Collisionless nonideal ballooning modes

Robert G. Kleva and Parvez N. Guzdar

Institute for Plasma Research, University of Maryland, College Park, Maryland 20742-3511

The nonzero inertia of the electron is shown to destabilize pressure-driven ballooning modes in collisionless tokamak plasmas that are stable in the ideal magnetohydrodynamic (MHD) approximation. The effect of the electron mass is characterized by the collisionless electron skin depth $d_e = c/\omega_{pe}$, where $\omega_{pe} = \sqrt{4\pi n e^2/m_e}$ is the electron plasma frequency. The growth rate of electron inertia ballooning modes increases with the magnitude of d_e, and also with the magnitude of the ratio β of the plasma thermal pressure to the pressure in the confining magnetic field. © *1999 American Institute of Physics.* [S1070-664X(99)00501-7]

I. INTRODUCTION

The most important limitation on the performance of large tokamaks is that imposed by disruptions. The fusion power output from a hot, magnetically confined plasma increases as the square of the ion density, while the energy input required to contain the particles rises with the strength of the confining magnetic field. Therefore, the ratio β of the plasma thermal pressure to the magnetic field pressure is an important figure of merit characterizing a tokamak's performance as a fusion reactor. Attempts to improve tokamak performance by increasing β are thwarted by disruptions. Tokamak discharges can operate stably only at values of β below a critical limit β_{crit}.[1-3] When β exceeds this limiting value, then there is a sudden, catastrophic loss of confinement.[3]

Most theoretical and computational analyses of tokamak stability at high β are based on the ideal magnetohydrodynamic (MHD) equations. A representative sample of ideal MHD analyses of tokamak stability is given in Refs. 4–10. These analyses do indeed show that, in the ideal MHD approximation, there is a linear stability limit in β. The plasma is stable for values of β smaller than some β_{ideal}, where the magnitude of β_{ideal} depends on the details of the toroidal plasma configuration, whereas the plasma is ideally unstable when $\beta > \beta_{\text{ideal}}$. Experimental observations have verified that tokamak discharges cannot be operated stably at values of β larger than the ideal limit β_{ideal}. However, these observations also show that tokamak plasmas can also be unstable to major β disruptions when $\beta < \beta_{\text{ideal}}$, contrary to the predictions of ideal MHD.[1,2] Typically, the experimentally determined limit in β, β_{crit}, is roughly one-half the limit β_{ideal} predicted by linear ideal MHD calculations. Furthermore, for values of $\beta < \beta_{\text{crit}}$ tokamaks experience minor β disruptions that exhibit the same characteristics as major β disruptions, but are less violent so that the plasma can recover without termination of the discharge.[3]

Since tokamak plasmas are observed to be unstable at values of $\beta < \beta_{\text{ideal}}$, nonideal effects in Ohm's law may have an important impact on stability. The electrical resistance of the plasma, caused by binary Coulomb collisions of the current carrying electrons with the ions, is known to destabilize

ballooning modes.[11-14] Since this classical collisional transport of the current destabilizes ballooning modes, small scale turbulence has been proposed as a destabilization mechanism through the generation of a turbulent current diffusion.[15] When $\beta \ll \beta_{\text{ideal}}$, classical resistive ballooning modes with moderate toroidal mode number n are either stable or only weakly unstable with a small growth rate. But for larger ß closer to β_{ideal} in magnitude, but still smaller, moderate n resistive ballooning modes grow much more rapidly. For a large tokamak with parameters given in Table I (major radius $R_0 = 260$ cm, minor radius $a = 80$ cm, toroidal magnetic field $B_\phi = 40$ kG, central temperature $T = 10$ keV, and plasma density $n = 5 \times 10^{13}$ cm^{-3}), the electron-ion collision time $\tau_{ei} \approx 400\,\mu$s. Resistive MHD is valid for time scales much longer than the electron-ion collision time. However, the thermal quench time in β limit disruptions is observed to be from 100 to 400 μs.[3] Furthermore, just prior to the thermal quench rapidly growing moderate n fluctuations are often seen, with a growth time that can be less than 50 μs.[3] Thus, the growth time of the precursors to β limit disruptions and the thermal quench time are less than an electron-ion collision time. As a consequence, collisions in the hot central plasma cannot play a role in β limit disruptions.

However, a collisionless plasma is not an ideal plasma, because the nonzero mass of the electrons is neglected in the ideal MHD approximation. Electron inertia has been found to play an important role both in collisionless magnetic reconnection,[16-18] and in the generation of magnetic fields by a collisionless dynamo.[19] In this paper we investigate the stability of collisionless, high β tokamak plasmas, retaining the physics of the nonzero electron mass. We find that electron inertia destablizes ballooning modes with moderate toroidal mode number n in tokamak plasmas that are stable in the ideal MHD approximation. Thus, even collisionless tokamak plasmas below the ideal β limit, $\beta < \beta_{\text{ideal}}$, are unstable because of the nonzero electron mass. The effect of the electron inertia is characterized by the collisionless electron skin depth $d_e = c/\omega_{pe}$, where $\omega_{pe} = \sqrt{4\pi n e^2/m_e}$. The growth rate γ of electron inertia ballooning modes increases with the magnitude of d_e. The growth rate also becomes larger as the

TABLE I. Tokamak parameters.

R_0	260 cm
a	80 cm
B_ϕ	40 kG
T	10 keV
n	5×10^{13} cm^{-3}

toroidal mode number n increases, as well as when β increases.

In Sec. II we extend the MHD equations to include the nonzero mass of the electrons in Ohm's law. We show that the electron mass manifests itself in the induction equation for the magnetic field through the collisionless electron skin depth. The high β equilibria used in our stability analysis are described in Sec. II. For the purpose of comparison, we first consider the ideal and resistive linear stability of these equilibria in the MHD approximation, neglecting the electron mass, in Sec. III. Then, in Sec. IV, the effect of electron inertia on the stability of ballooning modes is studied. The dependence of the growth rate γ on the magnitude of the electron skin depth is investigated. In addition, the functional dependence of γ on β, the toroidal mode number n, and the viscosity is also presented. The potential impact of these modes on the stability of high β tokamaks is discussed in Sec. V.

II. EQUATIONS AND EQUILIBRIUM

The MHD equations are a set of coupled equations for the magnetic field $\mathbf{B}$, mass velocity $\mathbf{V}$, pressure P, and mass density ρ_m. The time rate of change of the magnetic field is given by Faraday's induction equation

$$\frac{\partial \mathbf{B}}{\partial t} = -c \boldsymbol{\nabla} \times \mathbf{E}, \tag{1}$$

where the electric field $\mathbf{E}$ is determined by Ohm's law. Ohm's law, including the non-zero electron mass m_e as well as the resistivity η, is given by[20]

$$\mathbf{E} + \frac{\mathbf{V} \times \mathbf{B}}{c} = \frac{m_e}{ne^2} \left(\frac{\partial \mathbf{J}}{\partial t} + \boldsymbol{\nabla} \cdot (\mathbf{VJ} + \mathbf{JV}) \right) + \eta \mathbf{J}, \tag{2}$$

where the plasma current $\mathbf{J}$ is obtained from Ampere's law,

$$\boldsymbol{\nabla} \times \mathbf{B} = 4\pi \mathbf{J}/c. \tag{3}$$

Combining Eqs. (1)–(3), we obtain the generalized induction equation including the nonzero electron mass,

$$\frac{\partial \mathbf{B}}{\partial t} = \boldsymbol{\nabla} \times (\mathbf{V} \times \mathbf{B}) + d_e^2 \left(\frac{\partial \boldsymbol{\nabla}^2 \mathbf{B}}{\partial t} - \frac{4\pi}{c} \boldsymbol{\nabla} \times [\boldsymbol{\nabla} \cdot (\mathbf{VJ} + \mathbf{JV})] \right)$$
$$+ \frac{\eta c^2}{4\pi} \boldsymbol{\nabla}^2 \mathbf{B}, \tag{4}$$

where $d_e = c/\omega_{pe}$ is the electron skin depth with the electron plasma frequency $\omega_{pe} = \sqrt{4\pi ne^2/m_e}$. The nonzero electron mass appears in Eq. (4) only through the electron skin depth d_e. Suppose that the spatial variables, the magnetic field, and the mass density are normalized as follows: $L\boldsymbol{\nabla} \rightarrow \boldsymbol{\nabla}$,

$\mathbf{B}/B_0 \rightarrow \mathbf{B}$, and $\rho_m/\rho_{m0} \rightarrow \rho_m$. In terms of these normalizations L, B_0, and ρ_{m0}, we can define the Alfvén speed $V_A \equiv (B_0^2/4\pi\rho_{m0})^{1/2}$ and the Alfvén time $\tau_A \equiv L/V_A$. Then, making the replacements $t/\tau_A \rightarrow t$, $\mathbf{V}/V_A \rightarrow \mathbf{V}$, $P/(B_0^2/4\pi) \rightarrow P$, $4\pi L\mathbf{J}/B_0 c \rightarrow \mathbf{J}$, and $\eta c^2 \tau_A/4\pi L^2 \equiv \tau_A/\tau_r \equiv S^{-1} \rightarrow \eta$ with the resistive time $\tau_r \equiv 4\pi L^2/\eta c^2$ and the Lundquist number (magnetic Reynolds number) $S \equiv \tau_r/\tau_A$, the generalized Ohm's law (4) can be written in the following normalized form:

$$\partial(\mathbf{B} - d_e^2 \boldsymbol{\nabla}^2 \mathbf{B})/\partial t = \boldsymbol{\nabla} \times (\mathbf{V} \times \mathbf{B}) - d_e^2 \boldsymbol{\nabla} \times [\boldsymbol{\nabla} \cdot (\mathbf{VJ} + \mathbf{JV})]$$
$$+ \eta \boldsymbol{\nabla}^2 \mathbf{B}. \tag{5}$$

In these normalized units, the MHD equations for the momentum $\mathbf{U} \equiv \rho_m \mathbf{V}$, pressure, and mass density are[21]

$$\partial \mathbf{U}/\partial t + \boldsymbol{\nabla} \cdot (\mathbf{VU}) = \mathbf{J} \times \mathbf{B} - \boldsymbol{\nabla} P + \mu \boldsymbol{\nabla}^2 \mathbf{U}, \tag{6}$$

$$\partial P/\partial t + \boldsymbol{\nabla} \cdot (\mathbf{V} P) = 0, \tag{7}$$

$$\partial \rho_m/\partial t + \boldsymbol{\nabla} \cdot \mathbf{U} = 0, \tag{8}$$

where μ is the viscosity.

Consider toroidal geometry defined by coordinates (R,ϕ,z), where R is the distance from the major axis of the torus, z is the vertical distance along the major axis, and ϕ is the toroidal angle. Suppose that the plasma is surrounded by a toroidal, ideal conducting wall with a rectangular cross section in the poloidal plane, which is centered at $(R = R_0, z = 0)$ with a half-width given by a. At the conducting wall boundary, the normal component of the magnetic field is zero ($B_R = 0$ at $R = R_0 \pm a$, $B_z = 0$ at $z = \pm a$) and the flow velocity is zero.

The normalized MHD equations (5)–(8) are solved in this toroidal geometry on a Cartesian grid in R and z. Spatial derivatives are evaluated to fourth order in the grid spacing Δ while time stepping is second order accurate in the time step Δt with a leapfrog trapezoidal scheme. The number of grid points used in the $R-z$ plane is varied to ensure that the numerical results are insensitive to this number.

Axisymmetric equilibria, independent of the toroidal angle ϕ, are obtained dynamically[21] by solving the normalized MHD equations in two dimensions in the poloidal plane to obtain force balance: $\mathbf{J} \times \mathbf{B} = \boldsymbol{\nabla} P$. Equilibria are characterized by the magnitude of the peak central pressure $P_{\max}$ and the total poloidal magnetic flux $\Delta\psi$. The quantity $\Delta\psi/(aR_0)$ is a measure of the average poloidal magnetic field. In terms of $P_{\max}$ and $\Delta\psi$, we define the ratio $\beta_{\rm pol}$ of the plasma pressure to the poloidal magnetic field pressure as

$$\beta_{\rm pol} = P_{\max}/(\Delta\psi/aR_0)^2. \tag{9}$$

An example of an equilibrium with $\beta_{\rm pol} = 1$ is shown in Fig. 1. This figure is a plot of the pressure P (solid line) and the safety factor q (dashed line) profiles as a function of R through the mid-plane $z = 0$, for a torus with major radius $R_0 = 3$, minor half-width $a = 1$, and inverse aspect ratio $\epsilon \equiv a/R_0 = \frac{1}{3}$. The central safety factor $q_0 = 1.1$ at the magnetic axis, and q increases monotonically from the magnetic axis to the wall, which is a magnetic separatrix. Over the range in R where the pressure gradient is nonzero, the magnetic shear is significant because the q profile is changing significantly.
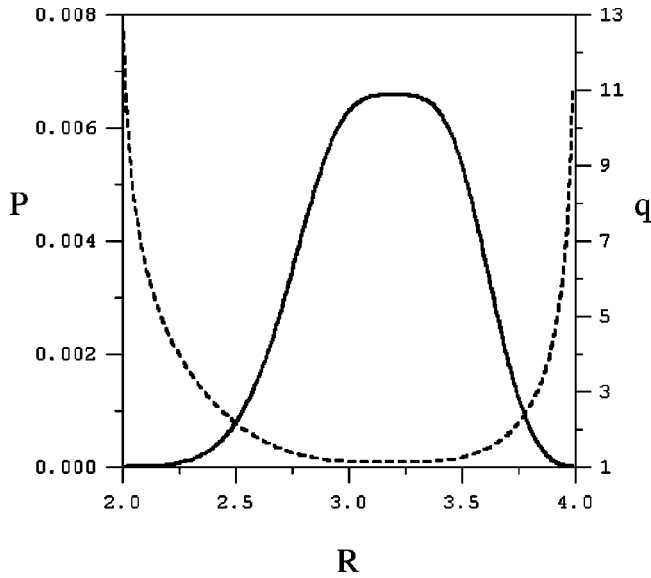
FIG. 1. Equilibrium. The pressure P (solid line) and the safety factor q (dashed line) are plotted versus the major radial coordinate R in the midplane ($z=0$), for an equilibrium with $\beta_{pol}=1$.

FIG. 2. Lundquist number. The growth rate γ is plotted as a function of the Lundquist number S for equilibria with $\beta_{pol}=1,2,3,4,5$. The points labeled by $S=\infty$ are obtained from the ideal MHD equations.

The normalized pressure is equal to $\frac{1}{2}\beta_{tor}$, where β_{tor} is the ratio of the peak plasma pressure to the pressure in the toroidal magnetic field. For the equilibrium shown in Fig. 1, $\beta_{tor}=1.3\%$. Equilibria with different values of β_{pol} are obtained by changing the peak pressure P_{max}.

Equations describing the stability of these equilibria to three-dimensional perturbations are obtained by linearizing Eqs. (5)–(8) about an equilibrium with a given pressure profile and current profile. All perturbed quantities are taken to vary in toroidal angle as $e^{-in\phi}$, where n is the toroidal mode number. For an arbitrary initial perturbation with mode number n, the linearized equations describing the perturbation are evolved in time. In the long-time asymptotic limit a normal mode forms in which the perturbation amplitude varies exponentially in time, $e^{\gamma t}$, where γ is the growth rate of the mode. Although both the equilibrium pressure and current are retained in the analysis, the gradient in the equilibrium pressure is the dominant source of instability.

III. IDEAL AND RESISTIVE BALLOONING MODES

For the purpose of comparison, let us first consider the ideal and resistive stability of high β_{pol} toroidal plasmas, neglecting the electron mass. Figure 2 is a plot of the growth rate γ, normalized to the Alfvén time τ_A, of an $n=10$ mode as a function of the Lundquist number $S=1/\eta$ when $d_e^2=0$ and $\mu=\eta$, for five equilibria with different β_{pol}. From the bottom of the figure, the curves are for equilibria with $\beta_{pol}=1, 2, 3, 4$, and 5. The actual data points are given by the solid circles in Fig. 2; the data points are connected by straight lines for ease of visualization. The points labelled by $S=\infty$ are for $\eta=\mu=0$. When $\beta_{pol}=5$, the growth rate of the $n=10$ mode is nearly independent of S and the mode is unstable in the ideal MHD approximation. The growth rate is quite large; the growth time is just a little more than $10\tau_A$. For the tokamak parameters given in the Table I, τ_A
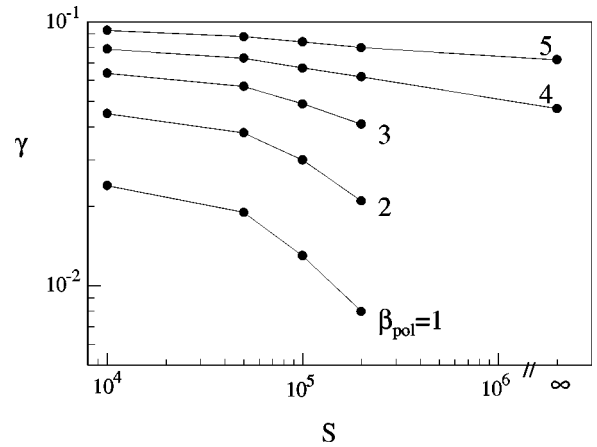
$\approx 0.1\ \mu$s. Thus, the growth time is only about $1\ \mu$s. As β_{pol} decreases, the magnitude of γ decreases and becomes increasingly dependent on the magnitude of η. When β_{pol} is reduced to 4, the mode is still unstable in the ideal MHD approximation. The lack of points at $S=\infty$ in Fig. 2 when $\beta_{pol}<4$ does not necessarily mean that the mode is stable in the ideal MHD limit. The dissipation in the equations damps grid scale noise in the simulations. When β_{pol} is reduced to 3, there is growing noise at the grid scale in the $\eta=\mu=0$ simulation, although a coherent mode structure still grows several orders of magnitude along with the grid scale noise. In addition to our full two-dimensional linear MHD code, we have also tested stability with a code that utilizes the ballooning approximation to solve the one-dimensional linear ballooning mode equation,[14] using the average pressure gradient over the region from $0.1P_{max}$ to $0.9P_{max}$ on the large R side of the magnetic axis in Fig. 1 where the two-dimensional structure of the modes is localized. The results from this code demonstrate that the $\beta_{pol}=3$ equilibrium is indeed ideally unstable, as is the $\beta_{pol}=2$ equilibrium, but the $\beta_{pol}=1$ equilibrium is not. Thus, the ideal stability limit, $\beta_{pol,ideal}$, lies in the range $1<\beta_{pol,ideal}<2$. As β_{pol} is reduced below the ideal limit, γ becomes increasingly dependent on the magnitude of S.

The dependence of the growth rate on the toroidal mode number is shown in Fig. 3. This figure is a plot of γ, normalized to τ_A, as a function of $\eta \equiv S^{-1}$ with $\mu=\eta$ in the $\beta_{pol}=1$ equilibrium, for three different mode numbers, $n=10$, 20, and 30. When $\eta=10^{-4}$, the $n=10$ mode is the fastest growing mode. But the growth rate of the $n=10$ mode decreases as η decreases. In contrast, the growth rate of the $n=20$ and 30 modes initially increase as η decreases below 10^{-4}. When η is reduced to 5×10^{-6}, the $n=30$ mode is the fastest growing of the three modes. For a given mode number n, the growth rate γ has a peak at $\eta=\eta_{max}(n)$, and the resistivity at the point of maximum growth $\eta_{max}(n)$ decreases as n increases. As we will show in the next section, the stabilizing influence of the viscosity is the cause of the decrease in γ for $\eta>\eta_{max}(n)$. In the large n one-dimensional ballooning mode equation, η and n appear
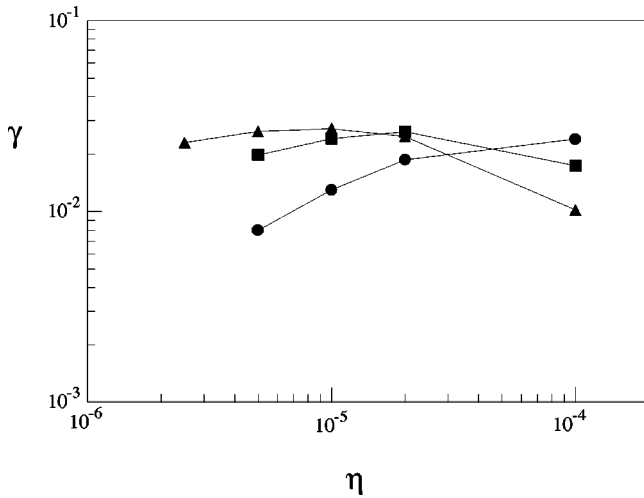
FIG. 3. Resistive ballooning mode. The growth rate γ is plotted as a function of the resistivity η for toroidal mode number $n=10$ (circles), 20 (squares), and 30 (triangles), for a plasma with $\mu=\eta$ and $\beta_{\mathrm{pol}}=1$.

only in the product ηn^2 and, therefore, γ is a function of ηn^2.[13] Similarly, the results of our two-dimensional simulations in Fig. 3 show that the peak in γ shifts to smaller η as n increases, and that the magnitude of the peak growth rate is nearly the same.

IV. ELECTRON INERTIA BALLOONING MODE

Resistive MHD is not a valid description of phenomena on time scales shorter than the electron-ion collision time. On such short time scales the plasma is collisionless, but not ideal because the mass of the electrons is nonzero. We now consider the stability of collisionless, high β_{pol} plasmas with $\eta=0$, but retain the effect of the non-zero electron mass.

In the generalized magnetic induction equation (5), the electron mass appears through the electron skin depth d_e. The effect of the electron mass on stability is shown in Fig.
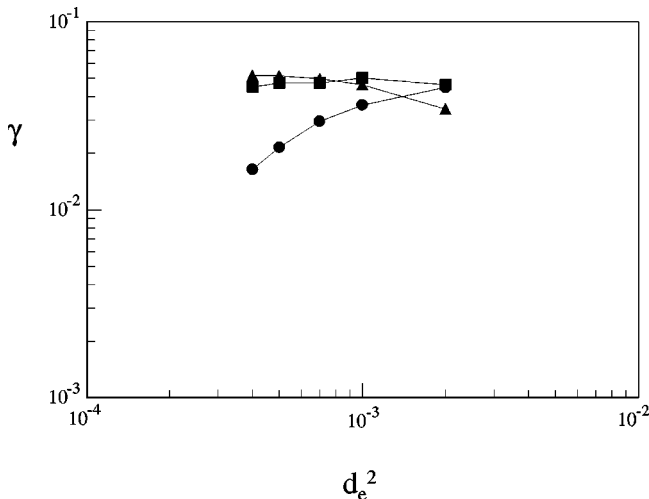

FIG. 4. Electron inertia ballooning mode. The growth rate γ is plotted as a function of the square of the collisionless electron skin depth d_e for toroidal mode number $n=10$ (circles), 20 (squares), and 30 (triangles), for a plasma with $\eta=0$, $\mu/d_e^2=10^{-2}$, and $\beta_{\mathrm{pol}}=1$.
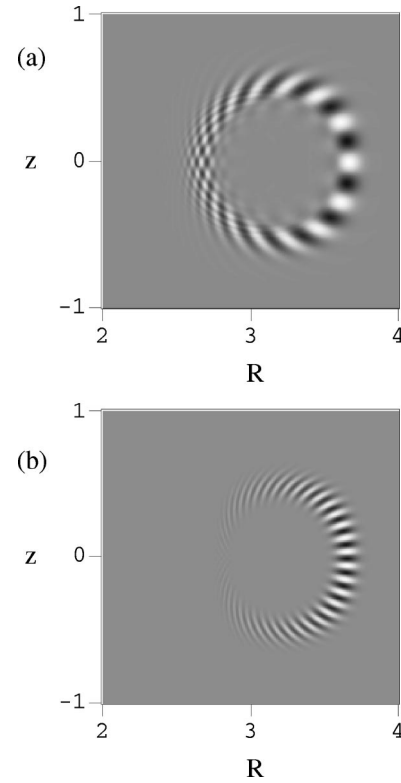

FIG. 5. Mode structure. The real part of the pressure perturbation in a $\beta_{\mathrm{pol}}=1$ equilibrium is plotted in the poloidal plane (R,z) for toroidal mode number (a) $n=10$ and (b) $n=30$, when $d_e^2=4\times10^{-4}$, $\eta=0$, and $\mu/d_e^2=10^{-2}$.

4. This figure is a plot of γ, normalized to τ_A, as a function of d_e^2 in the $\beta_{\mathrm{pol}}=1$ equilibrium with $\eta=0$ and $\mu/d_e^2=10^{-2}$, for three different toroidal mode numbers, $n=10$, 20, and 30. Qualitatively, the dependence of γ on d_e^2 in a collisionless plasma is similar to the dependence of γ on η is a collisional, resistive plasma. When $d_e^2=2\times10^{-3}$, the $n=10$ mode is the fastest growing mode. As d_e^2 decreases, γ decreases when $n=10$. In contrast, for the $n=20$ and 30 modes γ initially increases as d_e^2 decreases. When d_e^2 is reduced to 4×10^{-4}, the $n=30$ mode is the fastest growing mode. For a given mode number n, γ has a peak at $d_e^2=d_{e,\mathrm{max}}^2(n)$, and $d_{e,\mathrm{max}}^2(n)$ decreases as n increases. The peak growth rate is large; the growth time is only about 20 τ_A. The dominant effect of the electron mass comes from the time derivative term proportional to d_e^2 on the left-hand side of the induction equation (5); the term proportional to d_e^2 on the right-hand side of Eq. (5) affects the magnitude of γ by less than 5%.

The mode structure of the unstable modes is shown in Fig. 5. The real part of the pressure perturbation of the $n=10$ mode when $d_e^2=4\times10^{-4}$ is plotted in Fig. 5a, while the $n=30$ pressure perturbation is shown in Fig. 5b. The perturbation is positive in the lighter areas and negative in the darker ones. In both cases, the perturbation is localized on the pressure gradient on the large major radius (bad magnetic curvature) side of the magnetic axis, but the perturbation becomes more localized as n increases. This localization is characteristic of pressure driven ballooning modes.
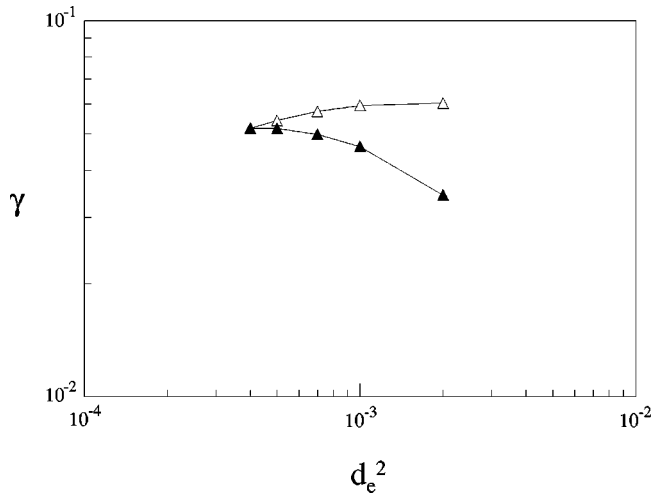
FIG. 6. Electron skin depth. The growth rate γ for an $n=30$ mode is plotted as a function of the square of the collisionless electron skin depth d_e for constant viscosity $\mu=4\times10^{-6}$ (open triangles), and μ proportional to d_e^2 (solid triangles), when $\eta=0$ and $\beta_{\text{pol}}=1$.

The decrease in γ at large d_e^2 in Fig. 4 for the $n=30$ mode is caused by the stabilizing influence of the increasing viscosity. As d_e^2 increases in Fig. 4, μ also increases so that the ratio μ/d_e^2 remains fixed at 10^{-2}. The dependence of γ on d_e^2 at fixed μ is shown in Fig. 6. The solid triangles are the results from Fig. 4 for $n=30$ when μ changes in proportion to d_e^2, while the variation in γ with fixed $\mu=4\times10^{-6}$ is given by the open triangles. When μ is fixed, the growth rate remains proportional to the magnitude of the electron skin depth. The effect of the viscosity on the stability of an $n=10$ electron inertia ballooning mode at fixed $d_e^2=4\times10^{-4}$ is shown in Fig. 7. As μ decreases, the growth rate increases and would apparently continue to increase if μ was further reduced.

All of the results presented so far are for a toroidal plasma with $\beta_{\text{pol}}=1$, a little below the ideal β limit. Figure 8 is a plot of the stability of equilibria with different β_{pol} to an $n=10$ perturbation when $d_e^2=1\times10^{-3}$. The perturbation is unstable for a wide range of β below the ideal limit. There is
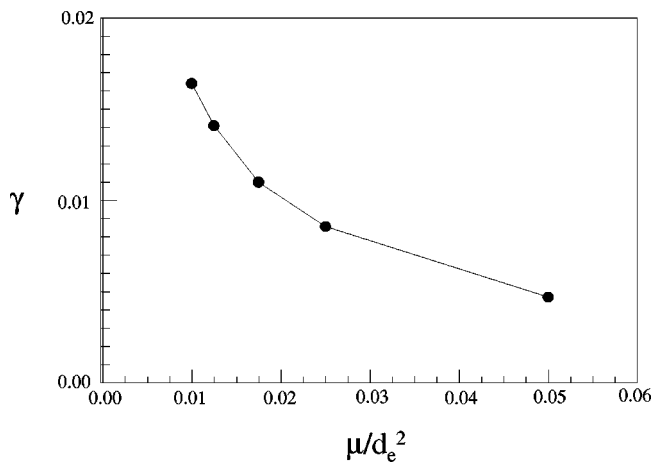

FIG. 7. Viscosity. The growth rate γ is plotted as a function of μ/d_e^2 for an $n=10$ mode when $d_e^2=4\times10^{-4}$, $\eta=0$, and $\beta_{\text{pol}}=1$.
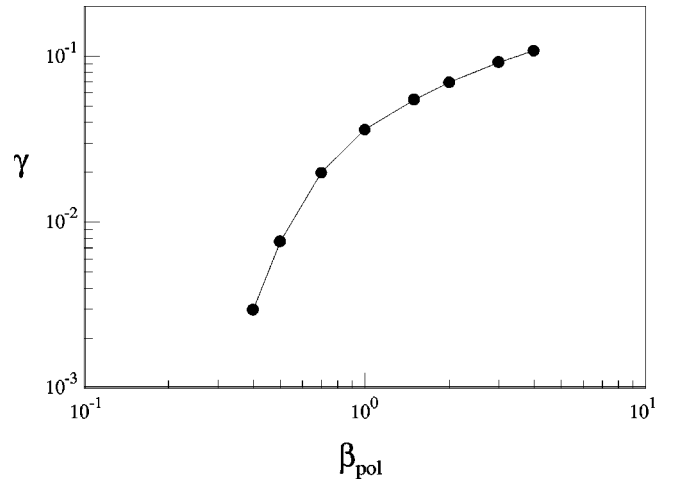

FIG. 8. β dependence. The growth rate γ is plotted as a function of β_{pol} for an $n=10$ mode when $d_e^2=10^{-3}$, $\eta=0$, and $\mu/d_e^2=10^{-2}$.

not an abrupt increase in γ as β_{pol} rises from below the ideal stability limit at $\beta_{\text{pol}}=1$ to above the ideal stability limit at $\beta_{\text{pol}}=2$. The growth rate decreases significantly as β_{pol} is reduced below $\beta_{\text{pol}}=1$, but the plasma is still unstable when $\beta_{\text{pol}}=0.4$, the smallest value of β_{pol} tested. Thus, an equilibrium with β approximately three times smaller than the ideal β limit is still linearly unstable because of the nonzero electron mass.

V. DISCUSSION

The nonzero inertia of electrons has been shown to destabilize ballooning modes in collisionless tokamak plasmas, for values of β below the ideal stability limit.

A comparison of Fig. 4 with Fig. 3 shows that the destabilization of ballooning modes by the electron mass (d_e^2) in collisionless plasmas is qualitatively similar to the resistive destabilization by η in collisional plasmas. For the tokamak parameters given in Table I, the magnitude of the Lundquist number $S\sim7\times10^9$. For the data in Fig. 3 with $\beta<\beta_{\text{ideal}}$, S is more than four orders of magnitude smaller. There may very well be a large reduction in γ as S is reduced by a factor of more than 10^4. But more importantly, resistive MHD is not a valid description of phenomena, such as the thermal quench in β limit disruptions, that occur on time scales short compared to an electron-ion collision time.

Even in collisionless plasmas, however, ballooning modes are destabilized by the nonzero electron inertia. The growth rate of collisionless electron inertia ballooning modes is large; the peak growth rate in Fig. 4 is larger than $0.05\tau_A^{-1}$. For the tokamak parameters listed in Table I, the corresponding growth time is of the order of one microsecond. For these same tokamak parameters, the square of the electron skin depth $d_e^2\approx1\times10^{-6}$, a little more than two orders of magnitude smaller than the smallest value of d_e^2 used in the numerical results presented in Fig. 4. But even if γ in Fig. 4 decreases by two orders of magnitude when d_e^2 is two orders of magnitude smaller, the growth time would still be short, only about $100\,\mu$s, comparable to the thermal quench time in β limit disruptions. Furthermore, the viscosity used

in Fig. 4 is a stabilizing factor. The viscosity is nonzero in the results presented in Fig. 4 because this dissipation is necessary to damp grid scale noise in the simulations. For the tokamak parameters in Table I, the normalized collisional viscosity $\mu = \rho_i^2 / \tau_{ii} \sim 2 \times 10^{-11}$, where ρ_i is the ion gyroradius and τ_{ii} is the ion-ion collision time, and the ratio $\mu/d_e^2 \sim 2 \times 10^{-5}$, nearly three orders of magnitude smaller than the ratio $\mu/d_e^2 = 10^{-2}$ used in Fig. 4. The results in Fig. 7 demonstrate that γ increases significantly as μ/d_e^2 is reduced in magnitude. Moreover, the ion-ion collision time is longer than the electron-ion collision time by $\sqrt{M_i/m_e}$; $\tau_{ii} \sim 20\,m\mathrm{s}$ for the tokamak parameters in Table I. Thus, there is not any collisional transport of momentum (viscosity) perpendicular to the magnetic field lines because these electron inertia ballooning modes grow on time scales shorter than τ_{ii}.

The growth rate of the collisionless electron inertia ballooning mode decreases as β_{pol} is reduced below unity in Fig. 8. It may be that the mode becomes stable due to the influence of plasma compressibility when β is far enough below the ideal stability limit β_{ideal}, as is the case for resistive ballooning modes.[13] Nonetheless, the results in Fig. 8 demonstrate that electron inertia ballooning modes are linearly unstable if β is not too much smaller than β_{ideal}. The ultimate impact of these modes on confinement is determined by their nonlinear evolution and possible nonlinear saturation mechanisms.

ACKNOWLEDGMENTS

[1] Y. Nagayama, M. Yamada, S. A. Sabbagh, E. D. Fredrickson, J. Manickam, M. Bell, R. V. Budny, A. Cavallo, A. C. Janos, M. E. Mauel, K. M. McGuire, G. A. Navratil, and G. Taylor, Phys. Fluids B **5**, 2571 (1993).

[2] M. Kikuchi and the JT-60 Team, in *Plasma Physics and Controlled Nuclear Fusion Research 1994, in Proceedings of the 15th International Conference,* Seville (International Atomic Energy Agency, Vienna, 1995), Vol. I, p. 31.

[3] E. D. Fredrickson, K. McGuire, Z. Chang, A. Janos, M. Bell, R. V. Budny, C. E. Bush, J. Manickam, H. Mynick, R. Nazikian, and G. Taylor, Phys. Plasmas **2**, 4216 (1995).

[4] J. W. Connor, R. J. Hastie, and J. B. Taylor, Phys. Rev. Lett. **40**, 396 (1978).

[5] M. S. Chance, S. C. Jardin, and T. H. Stix, Phys. Rev. Lett. **51**, 1963 (1983).

[6] F. Troyon, R. Gruber, H. Saurenmann, S. Semenzato, and S. Succi, Plasma Phys. Controlled Fusion **26**, 209 (1984).

[7] J. Manickam, Nucl. Fusion **24**, 595 (1984).

[8] M. W. Phillips, A. M. M. Todd, M. H. Hughes, J. Manickam, J. L. Johnson, and R. R. Parker, Nucl. Fusion **28**, 1499 (1988).

[9] A. D. Turnbull, F. Yasseen, A. Roy, O. Sauter, W. A. Cooper, S. Nicli, and F. Troyon, Nucl. Fusion **29**, 629 (1989).

[10] C. G. Schultz, A. Bondeson, F. Troyon, and A. Roy, Nucl. Fusion **30**, 2259 (1990).

[11] G. Bateman and D. B. Nelson, Phys. Rev. Lett. **41**, 1804 (1978).

[12] H. R. Strauss, Phys. Fluids **24**, 2004 (1981).

[13] J. F. Drake and T. M. Antonsen, Phys. Fluids **28**, 544 (1985).

[14] D. R. McCarthy, P. N. Guzdar, J. F. Drake, T. M. Antonsen, and A. B. Hassam, Phys. Fluids B **4**, 1846 (1992).

[15] K. Itoh, M. Yagi, S.-I. Itoh, A. Fukuyama, and M. Azumi, Plasma Phys. Controlled Fusion **35**, 543 (1993).

[16] J. A. Wesson, in *Plasma Physics and Controlled Nuclear Fusion Research 1990 in Proceedings of the 13th International Conference,* Washington (International Atomic Energy Agency, Vienna, 1991), Vol. II, p. 79.

[17] J. F. Drake and R. G. Kleva, Phys. Rev. Lett. **66**, 1458 (1991).

[18] M. Ottaviani and F. Porcelli, Phys. Rev. Lett. **71**, 3802 (1993).

[19] R. G. Kleva, Phys. Rev. Lett. **73**, 1509 (1994).

[20] N. A. Krall and A. W. Trievelpiece, *Principles of Plasma Physics* (McGraw-Hill, New York, 1973), p. 91.

[21] R. G. Kleva, Phys. Plasmas **3**, 2337 (1996).